

1
2 **ENSO Feedback Biases Common to Atmosphere-Ocean Coupled and Atmosphere-**
3 **Only Simulations of CMIP6 Climate Models**
4

5 **M. Hayashi¹**

6 ¹Earth System Division, National Institute for Environmental Studies, Tsukuba, Japan.
7
8

9 Corresponding author: Michiya Hayashi (hayashi.michiya@nies.go.jp)
10

11 **Key Points:**

- 12 • Atmospheric dynamic feedback of ENSO is biased common to the coupled and
13 uncoupled CMIP6 climate model simulations.
- 14 • In both simulations, the central Pacific zonal wind response to the equatorial precipitation
15 anomalies is too weak in boreal late winter.
- 16 • Simulating a peak-reduced and broad deep convective mean state is favorable for
17 enhancing the wind response and thus dynamic feedback.
18

19 Abstract

20 Climate models reproduce sea surface temperature (SST) variability of El Niño/Southern
21 Oscillation (ENSO) despite systematic feedback errors. Atmospheric feedback in response to
22 ENSO's SST anomalies remains biased even in atmosphere-only simulations, but the reason
23 therein is unclear. This study focuses on atmospheric internal processes to reveal ENSO
24 feedback biases common to the atmosphere-ocean coupled historical and atmosphere-only
25 simulations of CMIP6. The net heat flux feedback becomes comparable to observations once the
26 observed SST is prescribed, but the central Pacific zonal wind feedback is yet underestimated
27 albeit a realistic equatorial precipitation-SST relation. The wind feedback bias is attributed to the
28 wind responses to the equatorial precipitation anomalies that seasonally erroneously decline in
29 boreal late winter, common to both the coupled and atmosphere-only simulations. The model's
30 mean state with peak-reduced and broad deep convective areas is favorable for enhancing the
31 wind-precipitation relation and thus ENSO dynamic feedback.

32 Plain Language Summary

33 El Niño/Southern Oscillation (ENSO) is a key tropical Pacific atmosphere-ocean coupled
34 phenomenon for modulating year-to-year climate worldwide, of which sea surface temperature
35 (SST) variability is successfully simulated by the current generation of global climate models.
36 However, atmospheric feedback processes regarding the ENSO growth are systematically too
37 weak primarily due to too cold eastern equatorial Pacific SST in the atmosphere-ocean coupled
38 model simulations, potentially adding uncertainty in seasonal forecasts and future projections.
39 Such feedback bias remains even when observed SSTs drive the atmosphere-only models, but its
40 reason is yet elucidated. This study analyzed the state-of-the-art climate models and
41 observational datasets to reveal what characterizes the too-weak atmospheric feedback common
42 to the coupled and atmosphere-only models. The atmosphere-only models well simulate the
43 equatorial precipitation increase with warm eastern Pacific SST anomalies but systematically
44 underestimate the central Pacific westerly wind response to the increased equatorial
45 precipitation. The wind-precipitation relation erroneously declines in boreal late winter after
46 ENSO becomes matured, irrespective of the model types. To reduce the seasonal wind-
47 precipitation relation bias, the long-term averaged tropical precipitation in climate models needs
48 to have a reduced amplitude in the most convectively active area and be broadened toward
49 convectively suppressed areas.

50 1 Introduction

51 El Niño/Southern Oscillation (ENSO) is the dominant interannual mode driven by
52 equatorial Pacific atmosphere-ocean interactions and its large-scale circulation associated with
53 tropical precipitation variability modulates year-to-year climate worldwide (Philander, 1990; Jin,
54 1997; Timmermann et al., 2018). Most current atmosphere-ocean coupled climate models can
55 produce the observed amplitude of ENSO's sea surface temperature (SST) variability in the
56 equatorial Pacific and its remote teleconnection pattern (Planton et al., 2020; McGregor et al.,
57 2022), but the majority suffer from biased ENSO feedback for decades (Guilyardi et al., 2009,
58 2020; Kim et al., 2014; Bellenger et al., 2014; Bayr et al., 2020, hereafter BDL20; Hayashi et al.,
59 2020). The atmospheric part of ENSO feedback composes of key two dynamic and
60 thermodynamic processes: the positive zonal wind feedback and negative net heat flux feedback.
61 Both processes tend to be underestimated in climate models so that feedback errors are
62 compensated to each other, resulting in a seemingly realistic ENSO amplitude (Guilyardi et al.,

63 2009; Bayr et al., 2019). Too weak ENSO feedback causes a poor simulation of ENSO
 64 asymmetry (Hayashi et al., 2020; Bayr & Latif, 2022), which in turn affects the robustness of
 65 future projections of the ENSO amplitude and teleconnections under global warming (Cai et al.,
 66 2018, 2021; Bayr & Latif, 2022).

67 The too-weak ENSO feedbacks in coupled models are connected to too-cold eastern
 68 Pacific mean-state SST (excessive cold tongue) that shifts the Pacific Walker circulation to the
 69 west (BDL20). The cold tongue bias tends to be reduced by increasing the horizontal resolution
 70 of ocean models to better resolve eddy-driven heat transport (Wengel et al., 2021; Liu et al.,
 71 2022). In uncoupled atmospheric-only model simulations, where the SST is prescribed by
 72 observations, both dynamic and thermodynamic feedbacks are substantially improved from the
 73 corresponding coupled simulations, but their strength and related atmospheric circulation
 74 response remain too weak (BDL20; Wang et al., 2021). These circulation biases originate from
 75 atmospheric models and potentially induce erroneous ENSO dynamics in coupled models as
 76 well. However, it remains unclear whether there would be common feedback biases in both the
 77 coupled and uncoupled models.

78 This study analyzes ENSO feedback processes simulated by the state-of-the-art climate
 79 models participating in the Coupled Model Intercomparison Project phase 6 (CMIP6, Eyring et
 80 al., 2016) by focusing on atmospheric internal processes in atmosphere-ocean coupled and
 81 uncoupled simulations. As the atmospheric circulation responses are driven by condensation
 82 heating that accompanies precipitation, equatorial Pacific atmospheric responses to ENSO's SST
 83 anomalies (SSTAs) are separated into the precipitation response to the SST anomalies and
 84 atmospheric responses to the precipitation anomalies. This study further aims to reveal what
 85 characterizes the ENSO feedback biases originating from atmospheric models.

86 2 Data

87 Monthly outputs from the atmosphere-ocean coupled historical and atmosphere-only
 88 (Atmosphere Model Intercomparison Project, AMIP) runs of 32 CMIP6 climate models are
 89 analyzed. The historical and AMIP ensembles are composed of the first realizations represented
 90 as "r1" (Supplementary Table S1). Each model performance is not focused on since precisely
 91 evaluating ENSO feedback requires a large ensemble (Lee et al., 2021). For the observed SST,
 92 Centennial in situ Observation-Based Estimates of the Variability of SST and Marine
 93 Meteorological Variables version 2 (COBE-SST2, Hirahara et al., 2014) is used. The Global
 94 Precipitation Climatology Project version 3.2 (GPCP3, Huffman et al., 2022), Multi-Source
 95 Weighted-Ensemble Precipitation version 2.8 (MSWEP28, Beck et al., 2019), and CPC Merged
 96 Analysis of Precipitation (CMAP, Xie & Arkin, 1997) datasets are used for the observed
 97 precipitation. The atmospheric fields are derived from the fifth-generation ECMWF Reanalysis
 98 (ERA5, Hersbach et al., 2019a, 2019b) and the Japanese 55-year Reanalysis (JRA-55, Kobayashi
 99 et al. 2015). These datasets available for 1983-2014 are remapped to 2.5°N \times 2.5°E . The entire period
 100 is used to define climatology.

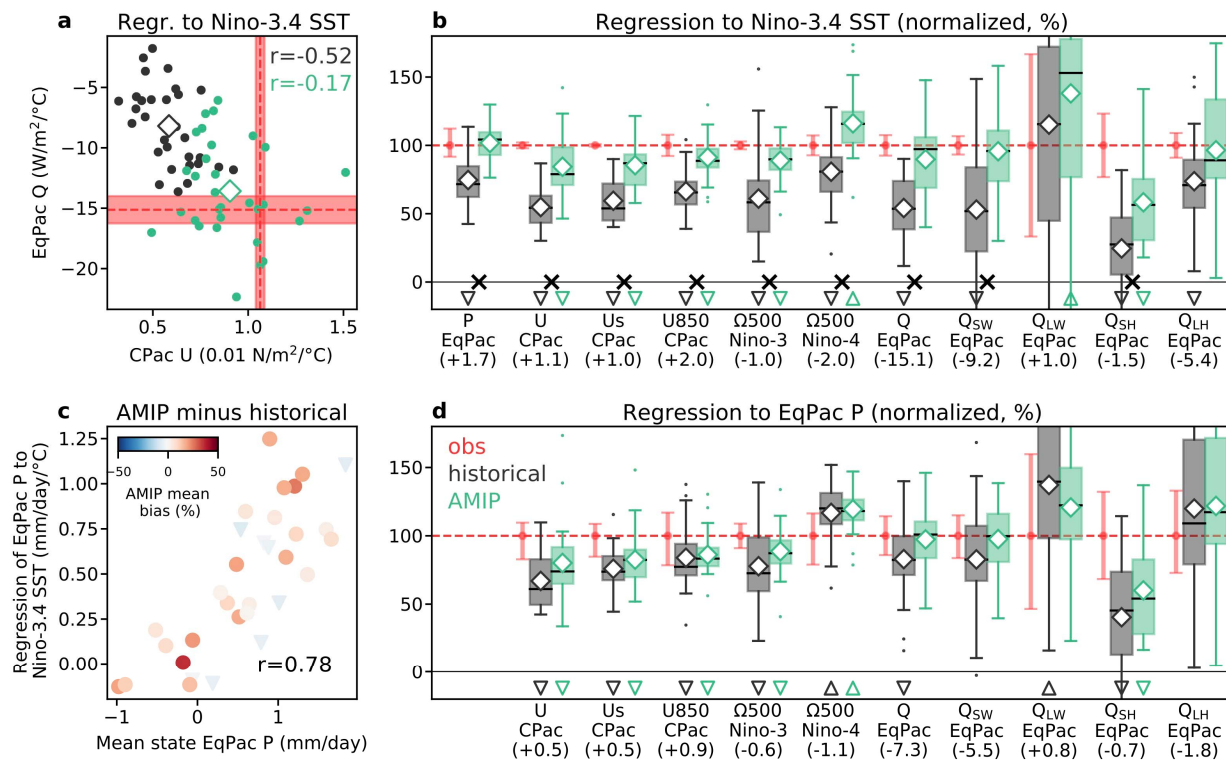
101 The Niño-3.4 (170°E - 150°W , 5°S - 5°N) SSTAs are used to characterize ENSO's SST
 102 variability. The zonal wind stress (U) and the zonal winds at the surface and 850 hPa (U_{s} and
 103 U_{850}) are averaged in the central Pacific domain (CPac; 150°E - 120°W , 5°S - 5°N), zonally wider
 104 than the Niño-4 region (160°E - 150°W , 5°S - 5°N) to broadly capture the equatorial wind
 105 responses. The vertical velocity at 500 hPa (Ω_{500}) is separately analyzed in the Niño-3 (150°W -

106 90°W, 5°S-5°N) and Niño-4 regions. The precipitation (P) is averaged in the Niño-3 and Niño-4
 107 combined equatorial Pacific domain (EqPac; 160°E-90°W, 5°S-5°N). The EqPac net surface heat
 108 flux (Q) and its surface shortwave (SW) and longwave (LW) radiative, sensible (SH), and latent
 109 (LH) heat flux components are also assessed.

110 **3 Results**

111 The simulated ENSO feedbacks are compared with observational values (Fig. 1a). In the
 112 historical runs, both the positive dynamic and negative thermodynamic feedbacks, defined as the
 113 CPac U and EqPac Q anomalies regressed onto the Niño-3.4 SSTAs, are highly uncertain and
 114 too weak in all models (55% and 54% on average relative to the observational means;
 115 Supplementary Table S2). As the two feedbacks are correlated among the models ($r=-0.52$), the
 116 underestimated positive feedback is compensated by the underestimated negative feedback. This
 117 error compensation is attributable to the cold tongue SST bias (BDL20). In the AMIP runs, both
 118 feedbacks are enhanced than the historical runs but still underestimated, as also seen in CMIP5
 119 (BDL20). The ensemble averages of the dynamic and thermodynamic feedbacks are 84% and
 120 90% of observations. Even though the SST is identically provided from observations and thus
 121 there is no error compensation between the two feedbacks in the AMIP runs, the intermodel
 122 spreads remain substantial. These results suggest that the atmospheric internal processes solely
 123 generate the ENSO feedback biases and uncertainties to a large extent.

124



125

126 **Figure 1.** Atmospheric responses to the Niño-3.4 SST and EqPac precipitation anomalies in the
 127 historical (black) and AMIP (green) ensembles compared with the observational averages and

128 min-max ranges (red). **(a)** Scatterplots of the dynamic (x-axis) and thermodynamic (y-axis)
 129 feedback coefficients. **(b)** Box-whisker plots of regression coefficients to the Niño-3.4 SSTAs
 130 normalized by the observational averages (numbers shown below the x-axis without the units).
 131 The up- and down-pointing triangles indicate that the historical and AMIP ensemble means are
 132 overestimated and underestimated significantly by the student's t-test and the cross marks
 133 represent the ensemble mean differences are significant by Welch's t-test at the 99% confidence
 134 levels. **(c)** Changes in the mean-state EqPac P and the P-SST relation from the historical to
 135 AMIP runs. Colors represent the mean-state EqPac P bias in the AMIP runs (% relative to the
 136 observational average). **(d)** Same as in b but for the regression to the EqPac P anomalies.
 137 Diamonds in a, b, and d show the ensemble means.

138

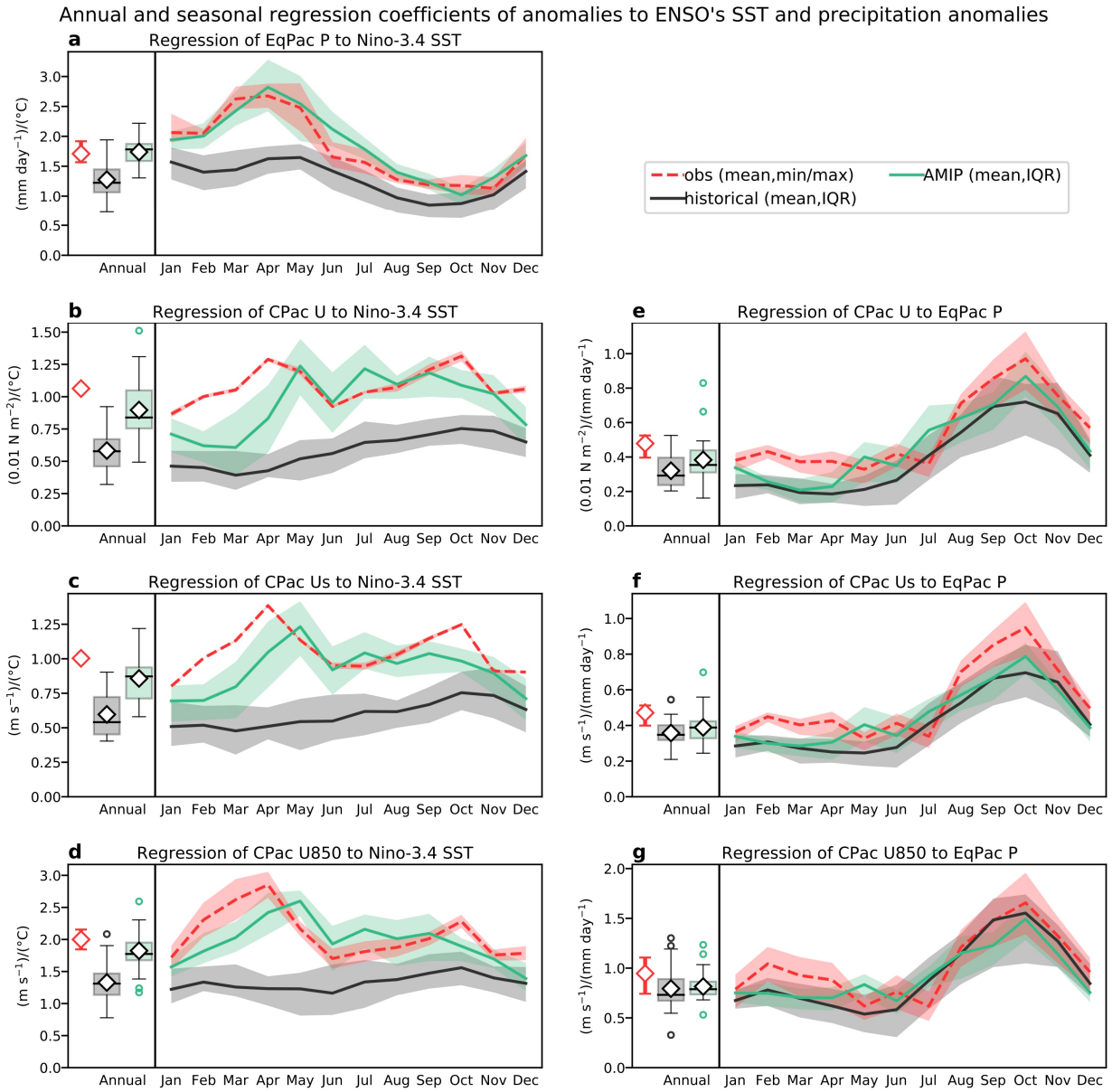
139 Various atmospheric responses to the Niño-3.4 SSTAs are examined (Fig. 1b). Here, each
 140 response is normalized by the observational average. The EqPac P anomalies regressed onto the
 141 Niño-3.4 SSTAs (hereafter, P-SST relation) are too weak in almost all the historical runs (75%
 142 on average), but the AMIP runs reproduce it consistent with observations (102%). The difference
 143 from the historical to AMIP ensembles is significant at the 99% confidence level, indicating the
 144 atmospheric models can reasonably simulate the P-SST relation. Indeed, the increments of the P-
 145 SST relation from the historical to AMIP runs are highly correlated with the mean-state EqPac P
 146 increments ($r=0.78$, Fig. 1c). Note that the higher increment of the mean-state precipitation does
 147 not correspond to the less biased climatology in the AMIP runs since there is no systematic
 148 relation between the increments and the AMIP mean-state biases (Fig. 1c). The dynamic
 149 feedback (hereafter, U-SST relation) and related circulation responses are significantly enhanced
 150 from the historical to AMIP runs (Fig. 1b). Similarly, the ensemble averages of the CPac Us and
 151 U850 responses are respectively changed from 59% and 66% (historical) to 85% and 91%
 152 (AMIP). The Niño-3 and Niño-4 Ω 500 responses are too weak in the historical runs (61% and
 153 81%) while both are enhanced in the AMIP runs (89% and 116%). Therefore, the circulation
 154 responses to the Niño-3.4 SSTAs are too weak even in the AMIP runs, except for the too-strong
 155 Niño-4 Ω 500 response. Meanwhile, the thermodynamic feedback and each component are
 156 significantly enhanced from the historical to AMIP runs, except for the LW and LH responses
 157 that have large intermodel uncertainties. In the AMIP runs, the SW and LH responses are close
 158 to observations on average. The SH response is too weak, and the LW response tends to be
 159 overestimated, but these are minor terms. Thus, the net thermodynamic feedback is not
 160 systematically biased once the mean-state SST bias is reduced.

161 Why the AMIP U-SST relation is systematically underestimated despite that the
 162 atmospheric models reasonably reproduce the P-SST relation? As this bias originates from the
 163 atmospheric models (Fig. 1b), the same issue may appear in the coupled simulations but
 164 potentially hidden behind the dominant mean-state biases. To confirm if this bias is common to
 165 the historical and AMIP runs, atmospheric responses to the EqPac P anomalies are examined
 166 (Fig. 1d). All the relationships in Fig. 1d are not significantly distinguished between the
 167 historical and AMIP runs, differently from Fig. 1b, indicating that their biases are common to
 168 both simulations. The CPac U anomalies regressed to the EqPac P anomalies (hereafter, U-P
 169 relation) are underestimated as well as the Us and U850 anomalies. On average, the U, Us, and
 170 U850 responses in the historical and AMIP runs are 67% and 80%, 76% and 83%, and 84% and
 171 86%, respectively. The Niño-3 Ω 500 responses are also too weak (78% and 89% in the historical

172 and AMIP runs, respectively) while the Niño-4 Ω 500 responses are too intense (117% and
173 119%). In contrast, the EqPac Q responses are close to observations on average in the AMIP runs
174 (97%) and not statistically different from those moderately underestimated in the historical runs
175 (83%). Two major components of the EqPac Q response, SW and LH, are not biased while the
176 SH component is underestimated and the LW component is moderately overestimated. As the
177 biased terms are minor, the CMIP6 atmospheric models reasonably reproduce the Q and P
178 relationship. In summary, the common issue for simulating ENSO in the CMIP6 coupled and
179 uncoupled models appears not in the thermodynamic feedback but in the dynamic feedback via
180 the underestimated U-P relation.

181 The seasonal biases related to the dynamic feedback are further examined in each
182 calendar month (Fig. 2). In observations, the P-SST relation is enhanced in boreal spring (March-
183 April-May, MAM) and suppressed in autumn (September-October-November, SON) and its
184 seasonal difference is as large as the annual estimate (Fig. 2a). The AMIP runs well reproduce its
185 amplitude and seasonal march. The historical runs also simulate a similar seasonality, but the P-
186 SST relation is too weak throughout the year. The observed U-SST relation has two moderate
187 peaks in MAM and SON (Fig. 2b). The MAM peak corresponds to the peak season of the P-SST
188 relation (Fig. 2a). In the historical runs, the U-SST relation is too weak regardless of the seasons.
189 The AMIP runs reproduce the observed amplitude of the U-SST relation from May to November
190 but fail to simulate it from December to April despite that the P-SST relation peaking in MAM is
191 comparable to observations. These results are also confirmed in Us and U850 (Fig. 2c,d). In a
192 similar manner, the seasonal dependence of the U-P relation is analyzed (Fig. 2e-g). The
193 observed amplitude becomes higher in July-December and suppressed in January-June (Fig. 2e).
194 This peak season corresponds to the SON peak of the U-SST relation (Fig. 2b). The seasonally
195 varying U-P relation is almost identical between the historical and AMIP runs and captures the
196 observed values during the peak season (SON). However, the simulated U-P relation is
197 substantially underestimated in boreal late winter (January-February-March, JFM). This bias is
198 also apparent in Us and U850 (Fig. 2f,g). Therefore, the underestimated U-P relation common to
199 the CMIP6 historical and AMIP runs (Fig. 1d) is attributable to the wind response biases in JFM.

200



201

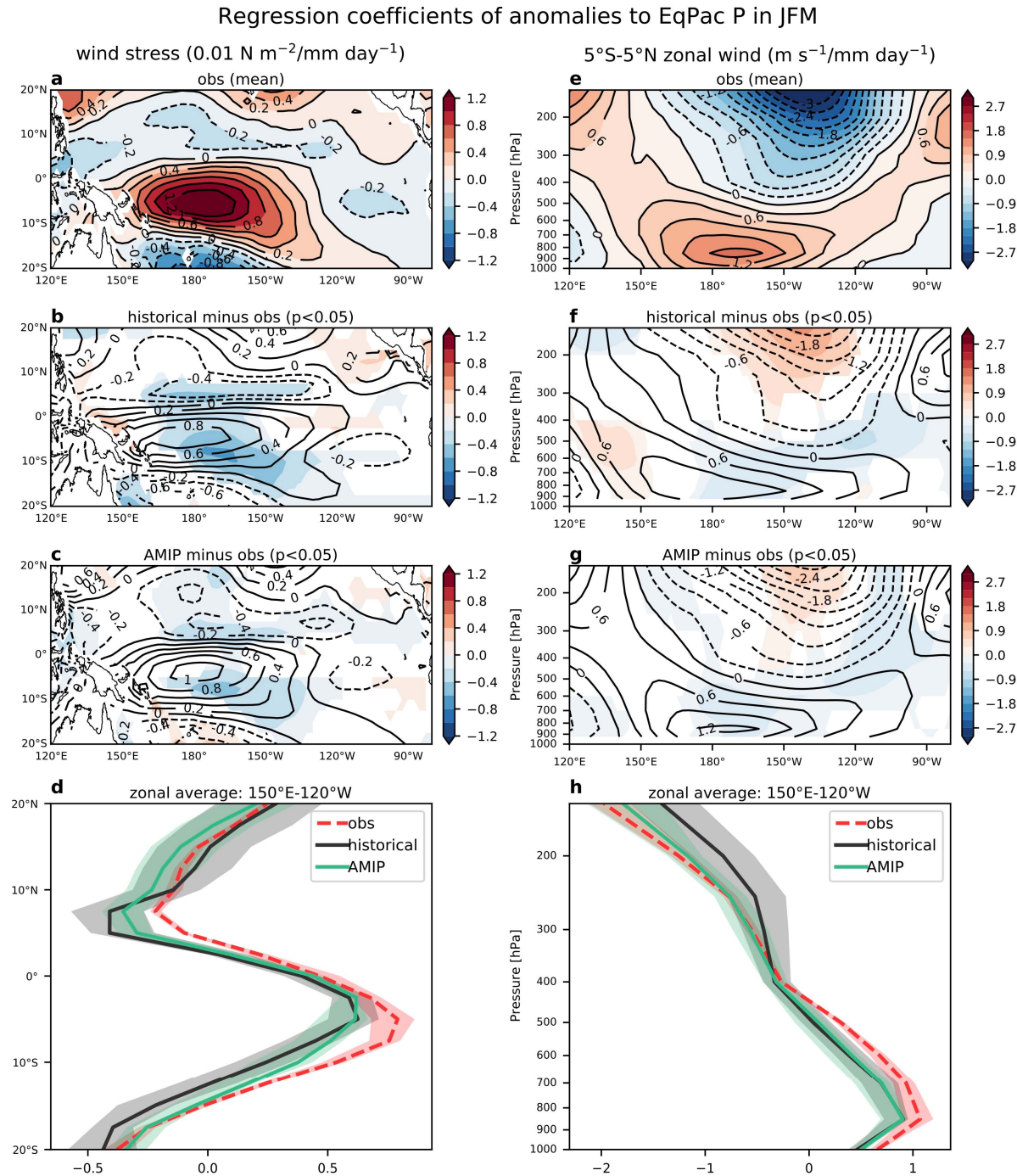
202 **Figure 2.** Seasonal dependence of the atmospheric responses to the Niño-3.4 SST and EqPac
203 precipitation anomalies in the historical (black) and AMIP (green) ensembles compared with the
204 observational averages and min-max ranges (red). The regression coefficients of the (a) EqPac P,
205 (b) CPac U, (c) CPac Us, and (d) CPac U850 anomalies to the Niño-3.4 SST anomalies. (e-g)
206 Same as in b-d but for the regression to the EqPac P anomalies. The lines with shading are the
207 ensemble averages and inter-quartile ranges in each calendar month. The annual plots are as in
208 Fig. 1 but with the units.

209

210 The spatial pattern biases of the JFM-averaged zonal wind responses to the EqPac P
211 anomalies are investigated (Fig. 3). In observations (Fig. 3a), the eastward (positive) wind stress

212 response is dominated along the equator, extended from 150°E to 120°W approximately and
213 shifted southward seasonally. The wind stress biases in both runs are significantly negative at the
214 northern and southern sides of the eastward wind responses (Fig. 3 b,c). The zonal-mean wind
215 stress response for 150°E-120°W shows that the simulated response is almost identical between
216 the historical and AMIP runs and is underestimated especially in the southern off-equator (Fig.
217 3d). Therefore, the central Pacific wind stress responses in the coupled and uncoupled models are
218 too weak and meridionally narrow. Figure 3 also demonstrates the model biases in the
219 tropospheric equatorial zonal wind responses. In both runs (Fig. 3f,g), the simulated wind
220 patterns are overall similar to observations (Fig. 3e), but the negative and positive biases are
221 significant over the central to eastern Pacific in the lower- and upper troposphere, respectively.
222 Despite that the historical runs suffer from the wind responses shifted westward due to the
223 excessive cold tongue (Fig. 3f), the CPac zonal wind response is similarly underestimated
224 through the lower troposphere in both historical and AMIP runs (Fig. 3h).

225



226

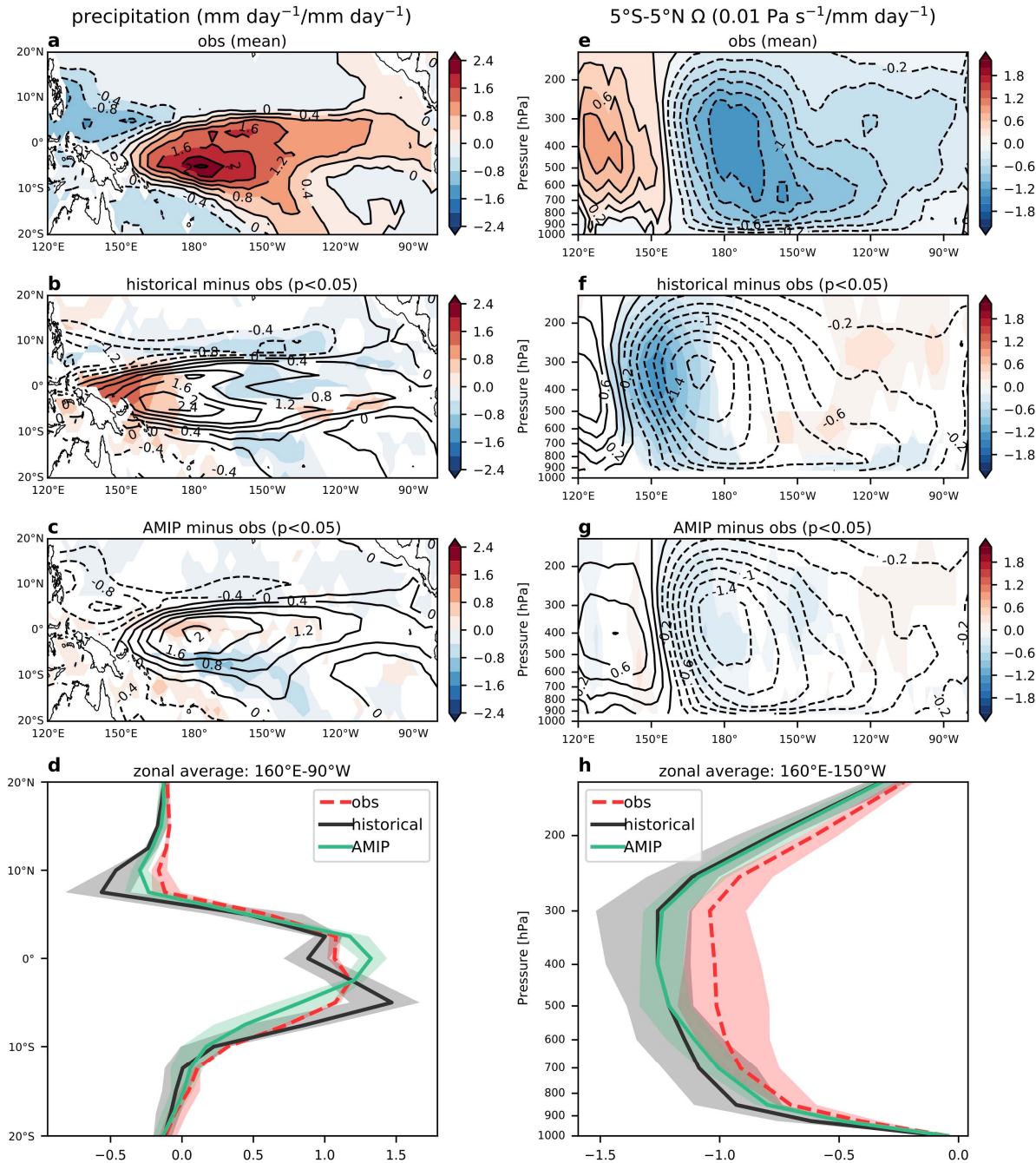
227 **Figure 3.** Regressed anomalies of the (left) zonal wind stress and (right) zonal wind between
228 $5^{\circ}\text{S}-5^{\circ}\text{N}$ to the EqPac precipitation anomalies in JFM. (a,e) Observational averages. (b,c,f,g)
229 Contours show the ensemble averages and shadings are the model biases relative to the
230 observational averages with $p < 0.05$ by the student's t-test. (d,h) Zonal averaged values between
231 150°E and 120°W . Shown are the observational averages and min-max ranges (red) and the
232 ensemble averages and interquartile ranges of the historical (black) and AMIP (green) runs.

233

The zonal wind biases in Fig. 3 are related to the P response patterns and equatorial Ω_{500} response profiles to the EqPac P anomalies (Fig. 4). The anomalous P pattern in JFM shows that the most active (positive) convective response near the dateline is shifted southward in observations (Fig. 4a), accompanied by the southward wind shift (Fig. 3a). In the AMIP runs (Fig. 4c,d), the active convective response over the central Pacific has its peak along the equator on average. Thus, the precipitation response tends to be suppressed in the southern off-equator from 3°S to 10°S to the east of the dateline but too strong near the equator. The equatorially confined precipitation anomalies drive the equatorial ascending (negative Ω_{500}) anomalies too intense in the central Pacific and too weak in the easternmost Pacific (Fig. 4e,g), therefore reducing the lower-tropospheric eastward and upper-tropospheric westward equatorial wind responses (Fig. 3g,h). In the historical runs (Fig. 4b,f), these equatorial P and Ω_{500} biases are not obvious due to the westward-shifted Walker circulation and also the too-intense climatological South Pacific convergence zone (Brown et al., 2020). Nevertheless, the tropospheric ascending responses are overestimated over the Niño-4 region to a similar extent to the AMIP runs (Fig. 4h) and also suppressed over the easternmost Pacific (Fig. 4f). Furthermore, the suppressed P response east to the dateline in the southern off-equator is significant in the historical runs as well (Fig. 4b,c). These biases are consistent with the reduced lower-tropospheric wind response (Fig. 3b,f).

252

Regression coefficients of anomalies to EqPac P in JFM



253

254 **Figure 4.** Regressed anomalies of the (left) precipitation and (right) vertical pressure velocity
 255 between 5°S-5°N to the EqPac precipitation anomalies in JFM. As in Fig. 3 but for the zonal
 256 averaged values between 160°E and 90°W in d and between 160°E and 150°W (CPac) in h.

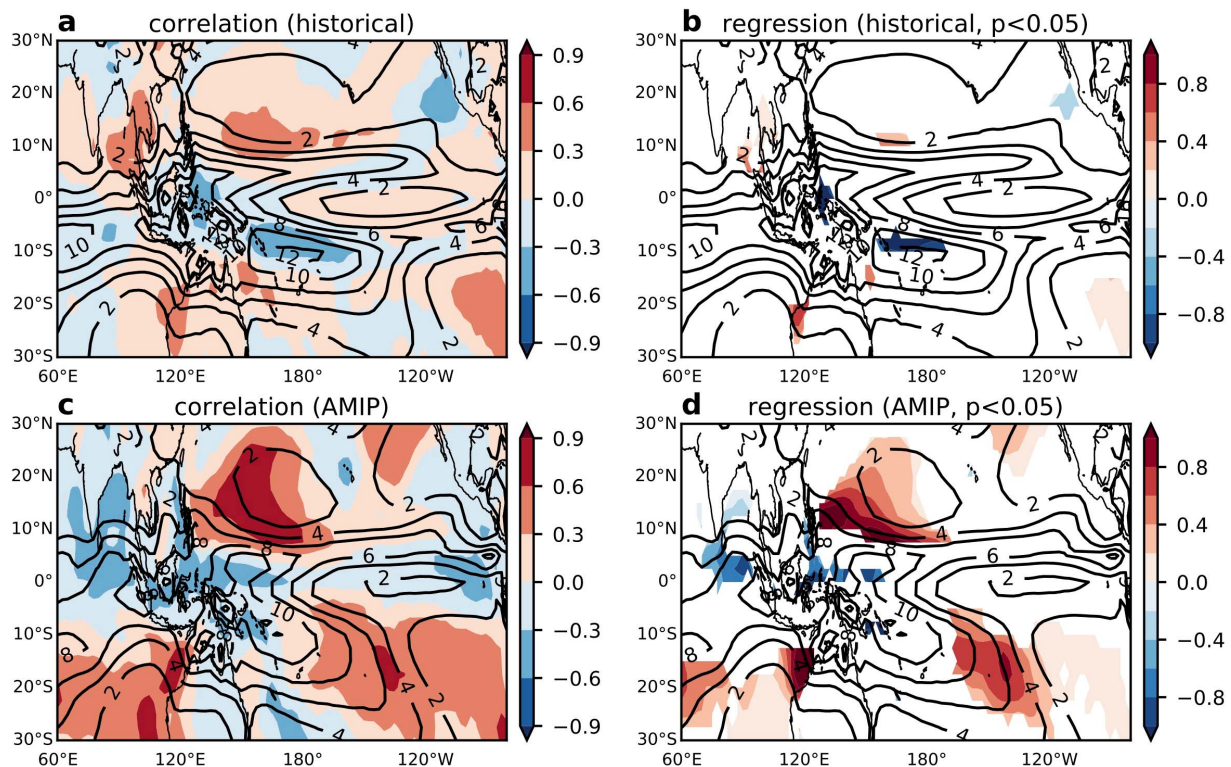
257

258 What controls the seasonal U-P relation bias in JFM? The intermodel correlation between
 259 the U-P relation and the mean-state tropical precipitation in each ensemble is negative over the

260 convectively active warm-pool region in the western Pacific while it is positive over the
 261 convectively suppressed off-equatorial areas such as the northwestern and southeastern Pacific
 262 (Fig. 5a,c). The AMIP intermodel regression coefficient map of the mean precipitation onto the
 263 normalized U-P relation (Fig. 5d) shows that the mean-state precipitation reduced over the warm
 264 pool and expanded to the northwestern and southeastern off-equatorial Pacific (“peak-reduced
 265 and broad” tropical deep convection) is preferable for enhancing the U-P relation. This peak-
 266 reduced and broad pattern is also recognized in the historical runs (Fig. 5a,b), despite their
 267 substantially biased mean-state SST and precipitation patterns. These results imply that tuning
 268 the model climatology to have less warm-pool precipitation and more descending area
 269 precipitation may increase the dynamic feedback.

270

Intermodel correlation between the mean precip. and U-P relation



271

272 **Figure 5.** Intermodel (left) correlation and (right) regression coefficients of the mean-state
 273 precipitation to the normalized U-P relation in JFM in the (top) historical and (bottom) AMIP
 274 runs. The contours indicate the ensemble mean of the mean-state precipitation in the historical
 275 and AMIP runs. (b,d) Shadings show the regression coefficients with $p < 0.05$.

276

277 4 Conclusions and discussion

278 This study analyzed the coupled historical and uncoupled AMIP simulations of CMIP6 to
 279 reveal what characterizes biases in the atmospheric ENSO feedback. Both the positive dynamic

and negative thermodynamic feedbacks are underestimated in the CMIP6 historical runs (Planton et al., 2021), but substantially increased in the CMIP6 AMIP runs as the observed SST produces higher mean-state precipitation and thus the equatorial precipitation anomalies in response to ENSO's SST variability (Fig. 1a-c). In the AMIP runs, the thermodynamic feedback becomes comparable to observations as the SW response is improved (Fig. 1b). However, the dynamic feedback represented by the central Pacific zonal wind response remains too weak in the majority of the CMIP6 AMIP runs (Fig. 1b), as in the former generation of climate models in CMIP5 (BDL20), despite that the equatorial precipitation response is not systematically biased. The underestimation of the AMIP dynamic feedback seasonally appears in boreal late winter and is attributed to too-weak zonal wind response to the equatorial precipitation anomalies, common to both the historical and AMIP runs (Figs. 1d and 2). The biased wind-precipitation relation coincides with equatorial ascending anomalies too weak over the eastern Pacific and too strong over the western Pacific and characterized by equatorially confined precipitation anomalies (Figs. 3 and 4). The model mean state with peak-reduced and broad deep convective areas is favorable for enhancing the wind-precipitation relation and thus the dynamic feedback (Fig. 5).

The underestimated dynamic feedback is a long-standing issue since the former generation of climate models. BDL20 found that in CMIP5 AMIP runs, the too-weak wind response to the Niño3.4 SSTAs may be increased by enhancing the Niño-4 Ω 500 response, which is already overestimated, as also confirmed in CMIP6 (Figs. 1 and 4). Thus, tuning models to enhance the Ω 500 response is not physically reasonable for improving the dynamic feedback. The seasonal bias needs to be focused on more when discussing the model's fidelity in atmospheric ENSO feedback as the too-weak wind response appears in the ENSO's peak and decaying season (boreal late winter) rather than its developing season (summer-autumn). In the late winter, many CMIP6 models fail to reproduce the seasonal southward wind shift albeit it is critical for the rapid decay of strong El Niño events and asymmetry of the ENSO life cycle (McGregor et al., 2012; Stuecker et al., 2013; Abellán & McGregor, 2016). The meridionally confined zonal wind anomalies may also affect the ENSO frequency as narrower wind anomalies are favorable for simulating a shorter period of ENSO (Kirtman, 1997; Capotondi et al., 2006; Lu et al., 2018). Improving the dynamic feedback may provide a more trustful projection of ENSO in a changing climate (Hayashi et al., 2020; Cai et al., 2021; Bayr & Latif, 2022), which needs to be confirmed in further studies.

311 Acknowledgments

312 This work was supported by JSPS KAKENHI Grant Number JP21K13993 and MEXT
313 KAKENHI Grant Number JPMXD0722680395.

314 Open Research

315 CMIP6 models used can be found in Table S1. The CMIP6 dataset is available at <https://esgf-node.llnl.gov/projects/cmip6/>, COBE-SST2 at <https://climate.mri-jma.go.jp/pub/ocean/cobe-sst2/>,
316 GPCP3 at <https://measures.gesdisc.eosdis.nasa.gov/data/GPCP/GPCPDAY.3.2/>, MSWEP28 at
317 <http://www.gloh2o.org/mswep/>, CMAP at <https://psl.noaa.gov/data/gridded/data.cmap.html>, ERA5 at
318 <http://www.gloh2o.org/era5/>

319 <https://doi.org/10.24381/cds.f17050d7> and <https://doi.org/10.24381/cds.6860a573>, and JRA-55 at
320 https://jra.kishou.go.jp/JRA-55/index_en.html. The data and scripts will be available on the figshare
321 repository.

322

323 **References**

- 324 Abellán, E., & McGregor, S. (2016). The role of the southward wind shift in both, the seasonal
325 synchronization and duration of ENSO events. *Climate Dynamics*, 47, 509–527.
326 <https://doi.org/10.1007/s00382-015-2853-1>
- 327 Bayr, T., Dommenget, D., & Latif, M. (2020). Walker circulation controls ENSO atmospheric
328 feedbacks in uncoupled and coupled climate model simulations. *Climate Dynamics*, 54,
329 2831–2846. <https://doi.org/10.1007/s00382-020-05152-2>
- 330 Bayr, T., & Latif, M. (2022). ENSO atmospheric feedbacks under global warming and their
331 relation to mean-state changes. *Climate Dynamics*. <https://doi.org/10.1007/s00382-022-06454-3>
- 333 Bayr, T., Wengel, C., Latif, M., Dommenget, D., Lübbecke, J., & Park, W. (2019). Error
334 compensation of ENSO atmospheric feedbacks in climate models and its influence on
335 simulated ENSO dynamics. *Climate Dynamics*, 53, 155–172.
336 <https://doi.org/10.1007/s00382-018-4575-7>
- 337 Beck, H. E., Wood, E. F., Pan, M., Fisher, C. K., Miralles, D. G., van Dijk, A. I. J. M., et al.
338 (2019). MSWEP v2 global 3-hourly 0.1° precipitation: methodology and quantitative
339 assessment. *Bulletin of the American Meteorological Society*, 100(3), 473–500.
340 <https://doi.org/10.1175/BAMS-D-17-0138.1>

- 341 Bellenger, H., Guilyardi, E., Leloup, J., Lengaigne, M., & Vialard, J. (2014). ENSO
342 representation in climate models: from CMIP3 to CMIP5. *Climate Dynamics*, 42, 1999–
343 2018. <https://doi.org/10.1007/s00382-013-1783-z>
- 344 Brown, J. R., Brierley, C. M., An, S.-I., Guarino, M.-V., Stevenson, S., Williams, C. J. R., *et al.*
345 (2020). Comparison of past and future simulations of ENSO in CMIP5/PMIP3 and
346 CMIP6/PMIP4 models. *Climate of the Past*, 16, 1777–1805. <https://doi.org/10.5194/cp-16-1777-2020>
- 348 Cai, W., Santoso, A., Collins, M., Dewitte, B., Karamperidou, C., Kug, J.-S., *et al.* (2021).
349 Changing El Niño–Southern Oscillation in a warming climate. *Nature Reviews Earth &*
350 *Environment*, 2, 628–644. <https://doi.org/10.1038/s43017-021-00199-z>
- 351 Cai, W., Wang, G., Dewitte, B., Wu, L., Santoso, A., Takahashi, K., *et al.* (2018). Increased
352 variability of eastern Pacific El Niño under greenhouse warming. *Nature*, 564, 201–206.
353 <https://doi.org/10.1038/s41586-018-0776-9>
- 354 Capotondi, A., Wittenberg, A., & Masina, S. (2006). Spatial and temporal structure of Tropical
355 Pacific interannual variability in 20th century coupled simulations. *Ocean Modelling*, 15,
356 274–298. <https://doi.org/10.1016/j.ocemod.2006.02.004>
- 357 Eyring, V., Bony, S., Meehl, G. A., Senior, C. A., Stevens, B., Stouffer, R. J., & Taylor, K. E.
358 (2016). Overview of the Coupled Model Intercomparison Project Phase 6 (CMIP6)
359 experimental design and organization. *Geoscientific Model Development*, 9, 1937–1958.
360 <https://doi.org/10.5194/gmd-9-1937-2016>
- 361 Guilyardi, E., Braconnot, P., Jin, F.-F., Kim, S. T., Kolasinski, M., Li, T., & Musat, I. (2009).
362 Atmosphere feedbacks during ENSO in a coupled GCM with a modified atmospheric

- 363 convection Scheme. *Journal of Climate*, 22(21), 5698–5718.
- 364 <https://doi.org/10.1175/2009JCLI2815.1>
- 365 Guiyadi, E., Capotondi, A., Lengaigne, M., Thual, S., & Wittenberg, A.T. (2020). ENSO
366 modeling: History, progress, and challenges. In M.J. McPhaden, A. Santoso and W. Cai
367 (Eds.), *El Niño Southern Oscillation in a Changing Climate, Geophysical Monograph
368 Series* (Vol. 253, pp. 201–226). Washington, DC: American Geophysical
369 Union. <https://doi.org/10.1002/9781119548164.ch9>
- 370 Hayashi, M., Jin, F.-F., & Stuecker, M. F. (2020). Dynamics for El Niño-La Niña asymmetry
371 constrain equatorial-Pacific warming pattern. *Nature Communications*, 11, 4230.
372 <https://doi.org/10.1038/s41467-020-17983-y>
- 373 Hersbach, H., Bell, B., Berrisford, P., Biavati, G., Horányi, A., Muñoz Sabater, J., et al. (2019a).
374 ERA5 monthly averaged data on single levels from 1959 to present, Copernicus Climate
375 Change Service (C3S) Climate Data Store (CDS), Accessed on 15 April 2022.
376 <https://doi.org/10.24381/cds.f17050d7>
- 377 Hersbach, H., Bell, B., Berrisford, P., Biavati, G., Horányi, A., Muñoz Sabater, J., et al. (2019b).
378 ERA5 monthly averaged data on pressure levels from 1959 to present, Copernicus Climate
379 Change Service (C3S) Climate Data Store (CDS), Accessed on 9 April 2021.
380 <https://doi.org/10.24381/cds.6860a573>
- 381 Hirahara, S., Ishii, M., & Fukuda, Y. (2014). Centennial-scale sea surface temperature analysis
382 and its uncertainty. *Journal of Climate*, 27, 57–75. [https://doi.org/10.1175/JCLI-D-12-00837.1](https://doi.org/10.1175/JCLI-D-12-
383 00837.1)
- 384 Huffman, G. J., Behrangi, A., Bolvin, D. T., & Nelkin, E. J. (2022). GPCP version 3.2 daily
385 precipitation data set, Goddard Earth Sciences Data and Information Services Center (GES

- 386 DISC), Accessed on 17 October
- 387 2022. <https://doi.org/10.5067/MEASURES/GPCP/DATA305>
- 388 Jin, F.-F. (1997). An equatorial ocean recharge paradigm for ENSO. Part I: Conceptual
389 model. *Journal of the Atmospheric Sciences*, 54(7), 811–829. [https://doi.org/10.1175/1520-0469\(1997\)054<0811:AEORPF>2.0.CO;2](https://doi.org/10.1175/1520-0469(1997)054<0811:AEORPF>2.0.CO;2)
- 390
- 391 Kim, S. T., Cai, W., Jin, F.-F., & Yu, J.-Y. (2014). ENSO stability in coupled climate models
392 and its association with mean state. *Climate Dynamics*, 42, 3313–3321.
393 <https://doi.org/10.1007/s00382-013-1833-6>
- 394 Kirtman, B. P. (1997). Oceanic Rossby wave dynamics and the ENSO period in a coupled
395 model. *Journal of Climate*, 10(7), 1690–1704. [https://doi.org/10.1175/1520-0442\(1997\)010<1690:ORWDAT>2.0.CO;2](https://doi.org/10.1175/1520-0442(1997)010<1690:ORWDAT>2.0.CO;2)
- 396
- 397 Kobayashi, S., Ota, Y., Harada, Y., Ebita, A., Moriya, M., Onoda, H., et al. (2015). The JRA-55
398 Reanalysis: General specifications and basic characteristics. *Journal of the Meteorological
399 Society of Japan*, 93, 5–48. <https://doi.org/10.2151/jmsj.2015-001>
- 400 Lee, J., Planton, Y. Y., Gleckler, P. J., Sperber, K. R., Guilyardi, E., Wittenberg, A. T., et al.
401 (2021). Robust evaluation of ENSO in climate models: How many ensemble members are
402 needed? *Geophysical Research Letters*, 48, e2021GL095041.
403 <https://doi.org/10.1029/2021GL095041>
- 404 Liu, B., Gan, B., Cai, W., Wu, L., Geng, T., Wang, H., et al. (2022). Will increasing climate
405 model resolution be beneficial for ENSO simulation? *Geophysical Research Letters*, 49,
406 e2021GL096932. <https://doi.org/10.1029/2021GL096932>
- 407 Lu, B., Jin, F.-F., & Ren, H.-L. (2018). A coupled dynamic index for ENSO periodicity. *Journal
408 of Climate*, 31(6), 2361–2376. <https://doi.org/10.1175/JCLI-D-17-0466.1>

- 409 McGregor, S., Cassou, C., Kosaka, Y., & Phillips, A. S. (2022). Projected ENSO teleconnection
410 changes in CMIP6. *Geophysical Research Letters*, 49,
411 e2021GL097511. <https://doi.org/10.1029/2021GL097511>
- 412 McGregor, S., Timmermann, A., Schneider, N., Stuecker, M. F., & England, M. H. (2012). The
413 effect of the South Pacific convergence zone on the termination of El Niño events and the
414 meridional asymmetry of ENSO. *Journal of Climate*, 25(16), 5566–5586.
415 <https://doi.org/10.1175/JCLI-D-11-00332.1>
- 416 Philander, S. G. (1990). *El Niño, La Niña, and the southern oscillation*. San Diego: CA,
417 Academic Press.
- 418 Planton, Y. Y., Guilyardi, E., Wittenberg, A. T., Lee, J., Gleckler, P. J., Bayr, T., et al. (2021).
419 Evaluating climate models with the CLIVAR 2020 ENSO metrics package. *Bulletin of the
420 American Meteorological Society*, 102(2), E193–E217. [https://doi.org/10.1175/BAMS-D-19-0337.1](https://doi.org/10.1175/BAMS-D-
421 19-0337.1)
- 422 Stuecker, M. F., Timmermann, A., Jin, F.-F., McGregor, S., & Ren, H.-L. (2013). A combination
423 mode of the annual cycle and the El Niño/Southern Oscillation. *Nature Geoscience*, 6,
424 540–544. <https://doi.org/10.1038/ngeo1826>
- 425 Timmermann, A., An, S.-I., Kug, J.-S., Jin, F.-F., Cai, W., Cobb, K., et al. (2018). El Niño-
426 Southern Oscillation complexity. *Nature*, 559, 535–545. [https://doi.org/10.1038/s41586-018-0252-6](https://doi.org/10.1038/s41586-
427 018-0252-6)
- 428 Wang, X.-Y., Zhu, J., Chang, C.-H., Johnson, N. C., Liu, H., Li, Y., et al. (2021).
429 Underestimated responses of Walker circulation to ENSO-related SST anomaly in
430 atmospheric and coupled models. *Geoscience Letters*, 8(17).
431 <https://doi.org/10.1186/s40562-021-00186-8>

- 432 Wengel, C., Lee, S.-S., Stuecker, M. F., Timmermann, A., Chu, J.-E., & Schloesser, F. (2021).
433 Future high-resolution El Niño/Southern Oscillation dynamics. *Nature Climate
434 Change*, 11, 758–765. <https://doi.org/10.1038/s41558-021-01132-4>
435 Xie, P., & Arkin, P. A. (1997). Global precipitation: A 17-year monthly analysis based on gauge
436 observations, satellite estimates, and numerical model outputs. *Bulletin of the American
437 Meteorological Society*, 78(11), 2539–2558. [https://doi.org/10.1175/1520-
439 0477\(1997\)078<2539:GPAYMA>2.0.CO;2](https://doi.org/10.1175/1520-
438 0477(1997)078<2539:GPAYMA>2.0.CO;2)